N89-24551

Pressure–strain-rate events in homogeneous turbulent shear flow

By JAMES G. BRASSEUR† AND MOON J. LEE‡

A detailed study of the intercomponent energy transfer processes by the pressure–strain-rate in homogeneous turbulent shear flow is presented. Probability density functions (pdf's) and contour plots of the rapid and slow pressure–strain-rate (π_{ij} and ϕ_{ij}) show that the energy transfer processes are extremely peaky, with high-magnitude events dominating low-magnitude fluctuations, as reflected by very high flatness factors (30–40) of the pressure–strain-rate.

The concept of the energy transfer class defined as

$$\mathbf{C}^{\pm\pm\pm} = \{\phi_{ij}(\mathbf{x},t)\,|\,\phi_{11} \gtrless 0, \phi_{22} \gtrless 0, \phi_{33} \gtrless 0\}$$

has been applied to investigate details of the direction as well as magnitude of the energy transfer processes. In incompressible flow, six disjoint energy transfer classes exist. Examination of contours in instantaneous fields, pdf's and weighted pdf's of the pressure–strain-rate indicates that in the low-magnitude regions (roughly $|\phi_{\alpha\alpha}| < 1.5$ r.m.s. $\phi_{\alpha\alpha}$) all six classes play an important role, but in the high-magnitude regions four classes of transfer processes, $\mathbf{C}^{++-}$, $\mathbf{C}^{-++}$, $\mathbf{C}^{-+-}$ and $\mathbf{C}^{--+}$, dominate. The contribution to the average slow pressure–strain-rate from the high-magnitude fluctuations is only 50% or less. The relative significance of high- and low-magnitude transfer events is discussed.

1. Introduction

We continue the analysis of the local intercomponent energy transfer process associated with the pressure–strain-rate correlation terms in the dynamic equation for the Reynolds-stress tensor, initiated in Brasseur & Lee (1987, hereafter referred to as BL). The work continues a program of enquiry into the kinematic structure and dynamic processes associated with local, random events underlying statistical quantities modeled in second-order closures. *Event* refers to a local concentration of the quantity in an instantaneous turbulent field. The aim is to describe classes of local events with similar characteristics, their interrelationships, and their relative kinematic and dynamic *significance*. Of particular interest is the structure and overall contribution of the most *powerful* events relative to the underlying low-level turbulent field.

The pressure–strain-rate term is the most controversial and least-understood term modeled in Reynolds-stress transport closures. Direct numerical simulations are

† The Pennsylvania State University
‡ Center for Turbulence Research

ideally suited to its study. The analysis begins with homogeneous turbulence in which pressure-induced intercomponent energy transfer may be unambiguously described by the correlation between fluctuating pressure p and strain-rate tensor $s_{ij} = \frac{1}{2}(u_{i,j} + u_{j,i})$. Homogeneous turbulent shear flow is analysed as a prototypical shear flow with turbulence production by mean shear. Significant structural and statistical similarities have been found between homogeneous shear flow and inhomogeneous wall-bounded flows (Kim *et al.* 1987; Lee *et al.* 1987; Rogers & Moin 1987).

Pressure (and accordingly pressure–strain-rate) is commonly decomposed into 'slow' and 'rapid' parts (see §2.1). In BL, both rapid and slow parts are discussed. Here, we shall concentrate on *slow pressure–strain-rate* events, and on a single realization in the asymptotic development of the flow.

2. Preliminary considerations

2.1. *Homogeneous turbulent shear flow*

The transport equation for the Reynolds stresses $R_{ij} = \overline{u_i u_j}$ in homogeneous turbulence may be written as

$$\frac{dR_{ij}}{dt} = P_{ij} + O_{ij} + T_{ij} - D_{ij}, \tag{1}$$

where $P_{ij} = -(S_{ik}R_{jk} + S_{jk}R_{ik})$ is the production rate, $O_{ij} = -(\Omega_{ik}R_{jk} + \Omega_{jk}R_{ik})$ the kinematic-rotation term and $D_{ij} = 2\nu\,\overline{u_{i,k}u_{j,k}}$ the (homogeneous) dissipation rate (see Lee & Reynolds 1985, §2.2 for a discussion). The pressure–strain-rate tensor $T_{ij} = \frac{2}{\rho}\,\overline{ps_{ij}}$ is the average value of the local product of fluctuating pressure and strain rate. Since the trace of the *instantaneous* pressure–strain-rate product ps_{ij} is zero in incompressible flow, ps_{ij} does not contribute to the production of turbulent energy. Thus, ps_{ij} may be interpreted as transferring turbulent energy locally, as well as globally, among components.

Our coordinate system for homogeneous turbulent shear flow with mean velocity $\mathbf{U} = (Sy, 0, 0)$ is sketched in figure 1 ($S = dU/dy$ is the mean shear rate). Turbulent shear flow with unidirectional mean velocity has the characteristic that the sum of turbulent energy production and energy transfer by mean rotation ($P_{ij} + O_{ij}$ in Eq. 1) increases component energy in the flow direction $\overline{u^2}$. Experimental measurements (Harris *et al.* 1977; Tavoularis & Corrsin 1981) and numerical simulations (Rogallo 1981; Rogers *et al.* 1986; Lee *et al.* 1987) suggest that homogeneous shear flow approaches an asymptotic-growth state in which the streamwise component $\overline{u^2}$ contains the most energy, followed by the spanwise component $\overline{w^2}$, then the normal component $\overline{v^2}$.

The present investigation makes use of the full simulation data of homogeneous shear flow (Rogers *et al.* 1986). The simulation was carried out by using the pseudospectral code developed by Rogallo (1981) with periodic boundary conditions on a deforming grid of $128 \times 128 \times 128$ nodes. Run R128 is analysed at total shear $St = 4$ and 8 (the largest scales approach the size of the computational domain

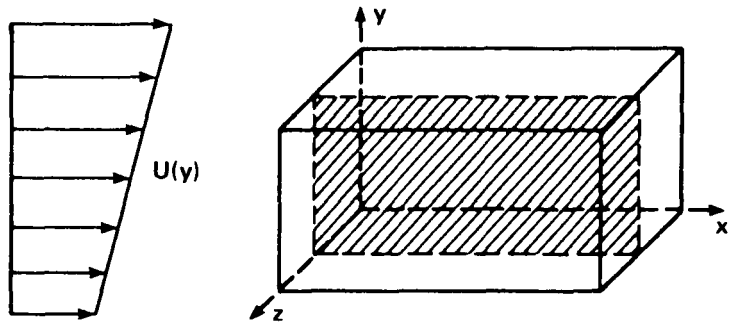

FIGURE 1. The subset of the computational domain and the xy-plane (hatched) over which the contours in figures 2 and 6 are shown. The spanwise location of the plane was arbitrarily chosen at the middle of the domain.

near $St = 16$). At $St = 8$, the Taylor-microscale Reynolds number is 74 and the dimensionless shear rate is $Sq^2/\epsilon = 8.8$ (where $q^2 = R_{ii}$ and $\epsilon = \frac{1}{2}D_{ii}$).

Corresponding to the two terms on the right hand side of the equation for fluctuating pressure in homogeneous shear flow

$$\frac{1}{\rho}\nabla^2 p = -2Su_{2,1} - u_{i,j}u_{j,i}, \tag{2}$$

pressure may be decomposed into two parts: $p = p_r + p_s$. The *rapid* pressure p_r responds directly to the mean shear, whereas the *slow* pressure p_s changes indirectly by the fluctuating velocities. *Instantaneous pressure–strain-rate* is accordingly separated into the rapid and slow parts:

$$\pi_{ij} = \frac{2}{\rho}p_r s_{ij} \quad \text{and} \quad \phi_{ij} = \frac{2}{\rho}p_s s_{ij}. \tag{3}$$

In BL, it was found that r.m.s. rapid pressure is approximately twice r.m.s. slow pressure from $St = 4$ to 8. The correlation coefficient between p_r and p_s, however, is very small, providing strong support for the modeling of the rapid and slow pressure–strain-rate terms separately (e.g. Lumley 1978). The lack of correlation between rapid and slow pressure is associated with a large difference in scale; p_r is contained within a very-large-scale, plane-wave-like structure, whereas p_s is concentrated in scales roughly corresponding to the 'energy-containing' eddies. Rapid and slow pressure–strain-rate, however, are only a factor of two different in scale, residing roughly within the 'energy-containing' range (vid. BL).

2.2. *Classes of the intercomponent energy transfer*

In order to explore the details of the physical processes in which turbulent kinetic energy is exchanged among components, we introduce the concept of *class* of the energy transfer processes. We discuss here only the slow pressure–strain-rate ϕ_{ij}, but the same technique has also been applied to the rapid term.

A *class of the intercomponent energy transfer* $\mathbf{C}^{s_1 s_2 s_3}$ is defined as the set of $\phi_{ij}(\mathbf{x}, t)$ with the same 'sign triplet' $(s_1 s_2 s_3)$ that are the signs of the intercomponent energy exchange, ϕ_{11}, ϕ_{22} and ϕ_{33}. There are six possible classes of the intercomponent energy transfer:†

$$\mathbf{C}^{\pm\pm\pm} = \{\phi_{ij}(\mathbf{x}, t) \,|\, \phi_{11} \gtrless 0, \phi_{22} \gtrless 0, \phi_{33} \gtrless 0\}. \tag{4}$$

For example, $\mathbf{C}^{-++}$ denotes the class of ϕ_{ij} in which energy leaves u ($\phi_{11} < 0$) and enters v and w ($\phi_{22} > 0$, $\phi_{33} > 0$). It may be noted that this classification is unique and the six classes are disjoint (or mutually exclusive).

The classification is used to quantify the contribution from each class to the average pressure–strain-rate. For this purpose, let $\phi_{ij}^{s_1 s_2 s_3}$ denote the values of the components of the instantaneous ϕ_{ij} that belong to class $\mathbf{C}^{s_1 s_2 s_3}$. Since the classes are disjoint, the average value of a pressure–strain-rate component is the sum of the contributions from the six classes for that component:

$$\Phi_{ij} = \overline{\phi_{ij}} = \sum_{s_1, s_2, s_3 = \pm} \Phi_{ij}^{s_1 s_2 s_3}, \tag{5}$$

where

$$\Phi_{ij}^{s_1 s_2 s_3} = \overline{\phi_{ij}^{s_1 s_2 s_3}}. \tag{6}$$

For example, Φ_{11}^{-++} represents the average value of all ϕ_{11}'s that belong to class $\mathbf{C}^{-++}$ ($\phi_{11} < 0$, $\phi_{22} > 0$ and $\phi_{33} > 0$).

By definition, Φ_{11}^{+++}, Φ_{11}^{++-} and Φ_{11}^{+--} are positive, and hence each represents energy transfer into u. The sum of these three positive parts represents the *total* energy transfer into u. The converse is true of the three negative contributions Φ_{11}^{-++}, Φ_{11}^{-+-} and Φ_{11}^{--+}. Thus, the average energy transfer rate in u may be decomposed as follows:

$$\Phi_{11} = \Phi_{11}^{+} + \Phi_{11}^{-}, \tag{7}$$

where

$$\Phi_{11}^{+} = \sum_{s_2, s_3 = \pm} \Phi_{11}^{+ s_2 s_3} = \Phi_{11}^{+++} + \Phi_{11}^{++-} + \Phi_{11}^{+--}, \tag{8a}$$

$$\Phi_{11}^{-} = \sum_{s_2, s_3 = \pm} \Phi_{11}^{- s_2 s_3} = \Phi_{11}^{-++} + \Phi_{11}^{-+-} + \Phi_{11}^{--+}. \tag{8b}$$

A similar decomposition can be obtained for the other components by appropriate permutation of the indices and sign triplets.

† (i) Classes $\mathbf{C}^{+++}$ and $\mathbf{C}^{---}$ are impossible in incompressible flow since $s_{ii} = 0$. (ii) The special cases with zero energy transfer in one, two or all components are ignored, since these occur very rarely in practice.

3. The local process of intercomponent energy transfer: slow term

3.1. *Spatial distribution of pressure–strain-rate*

Statistical averages of the instantaneous pressure–strain-rate terms π_{ij} and ϕ_{ij} show that energy is transferred out of the streamwise component u into the normal and spanwise components v and w, with w receiving the greater amount. At $St = 8$, the rapid and slow terms remove energy from u at the same rate. However, the *rapid* term transfers energy from u (and a lesser amount from v) into the *spanwise* component w, whereas the *slow* term transfers energy from u almost entirely into the *normal* component v (see BL).

As discussed in BL, however, analysis of the concentration of pressure–strain-rate events suggests a different, more complex process. We shall restrict the discussion to the slow term. Figure 2 shows contours of constant ϕ_{11}, ϕ_{22} and ϕ_{33} on the xy-plane shown in figure 1 (a 64×64 subset of the computational domain). The negative (solid) and positive (dashed) contours displayed are for $|\phi_{\alpha\alpha}| \geq 100$ (corresponding to 1.2–16.0 times the r.m.s. values). In this range, $\phi_{\alpha\alpha}$ is highly concentrated in relatively few (perhaps 30–40) powerful events over the computational domain.

The event labeled Ⓐ is the most powerful event in the computational domain (see BL for details). Here, it may be observed by overlaying the contours that energy is transferred locally from u, primarily to w and a little to v (small region of $\phi_{22} > 0$), and that w receives from v also. A similar process occurs in event Ⓑ. In event Ⓒ, energy leaves w to enter v; and in some parts of Ⓓ, energy is transferred from v to w, but from w to v in other parts.

In figure 3, a schematic is shown of the local energy transfer processes estimated by overlaying the contours in figure 2 and by classifying them into the six disjoint classes described in §2.2. Notice that the 'net' effect of energy transfer in the powerful events obtained by adding the contributions from the six classes is such that energy leaves u and enters v, consistent with the statistical averages. However, actual transfer processes are quite different. Among the possible six classes four classes of energy transfer are dominant (i.e. are associated with greatest amount of the energy transfer):

$$\mathbf{C}^{++-}, \quad \mathbf{C}^{-++}, \quad \mathbf{C}^{-+-}, \quad \mathbf{C}^{--+}. \tag{9}$$

Hence, the detailed processes underlying the net transfer (out of u into v) are such that energy is transferred from u primarily into w ($\mathbf{C}^{-++}$ and $\mathbf{C}^{--+}$), with v receiving most of its energy from w rather than from u ($\mathbf{C}^{-+-}$ and $\mathbf{C}^{++-}$).

3.2. *Probability density functions (pdf's)*

To characterize more quantitatively the local pressure–strain-rate events, a wide range of pdf's have been calculated. Comparison of pressure pdf's (not shown) with those in the log layer of a turbulent channel flow (J. Kim 1988, private communication) shows remarkable correspondence.

Pdf's $\mathsf{P}(\phi_{\alpha\alpha})$ of the diagonal components of ϕ_{ij} in standard form (scaled by the respective r.m.s. values ϕ'_{11}, ϕ'_{22}, ϕ'_{33}) are shown in figure 4; a Gaussian distribution is also plotted as a dotted line for reference. The flatness factors of ϕ_{11}, ϕ_{22}

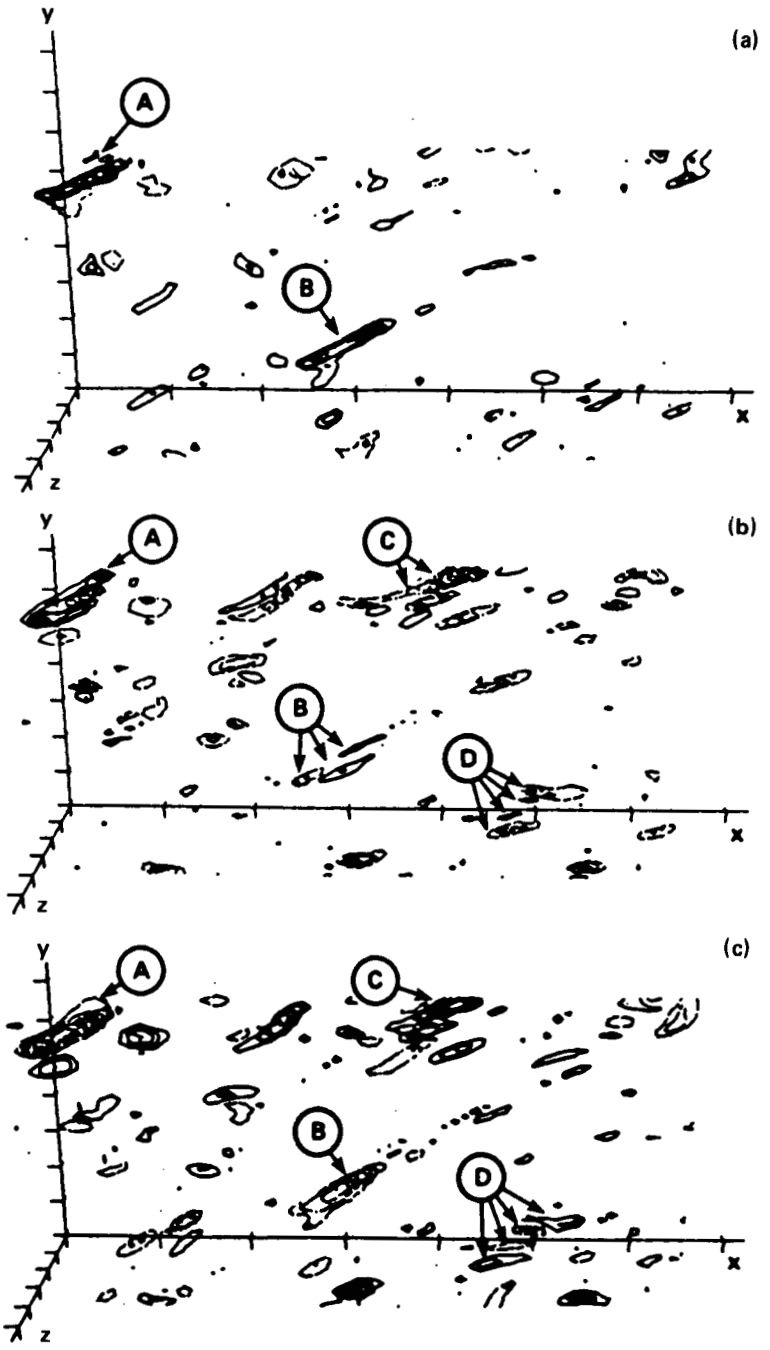

FIGURE 2. Contours of slow pressure–strain-rate on the xy-plane shown in figure 1 at $St = 8$: (*a*) ϕ_{11}; (*b*) ϕ_{22}; (*c*) ϕ_{33}. ——, negative; ----, positive. Four significant events are labeled (A), (B), (C) and (D).

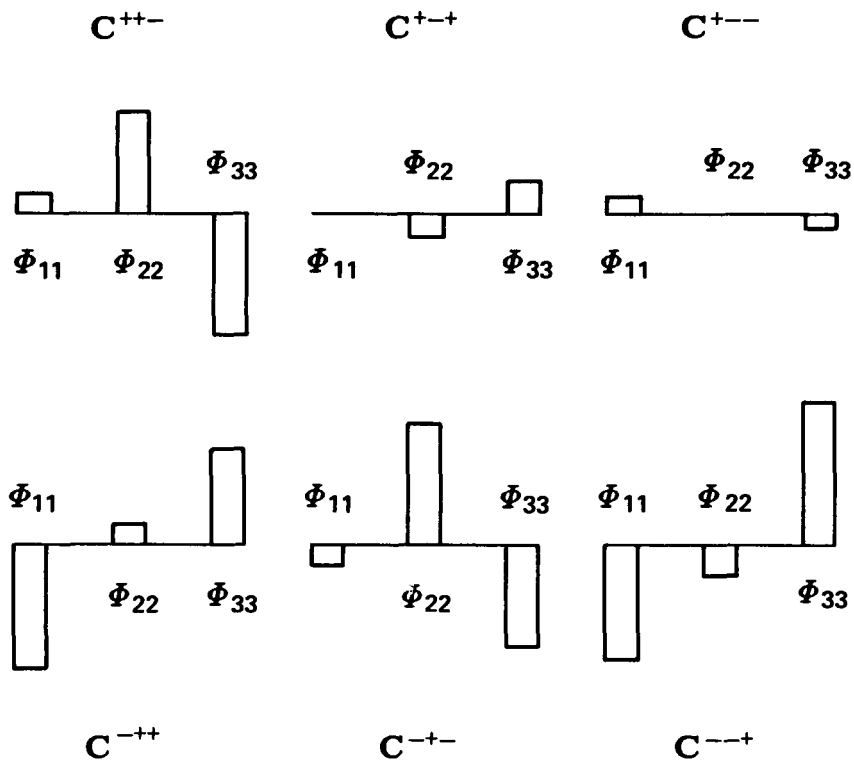

FIGURE 3. Schematic of the intercomponent energy transfer process, as deduced from contours of $\phi_{\alpha\alpha}$ in figure 2, shows that four transfer classes C^{++-}, C^{-++}, C^{-+-} and C^{--+} are dominant.

and ϕ_{33} are 41, 39 and 27, respectively. The high flatness factors, with the spikes in the pdf's near zero (see figure 4), are a reflection of the spottiness of the distribution of ϕ_{ij} with concentrated, high-magnitude events towering over a 'sea' of low-magnitude fluctuations. The skewness factors of ϕ_{11}, ϕ_{22} and ϕ_{33} are -3.9, 3.3 and 0.3, respectively. The high negative skewness factor of ϕ_{11} is indicative of dominance of negative events in the high-magnitude region; and the converse is true of ϕ_{22}. However, combination of the low skewness factor and high flatness factor of ϕ_{33} implies that high-level fluctuations of ϕ_{33} are relatively equally distributed on the both sides (figure 4*c*). These results are consistent with the deductions illustrated in figure 3.

The statistical average of the nth moment of a random variable ϕ is obtained by

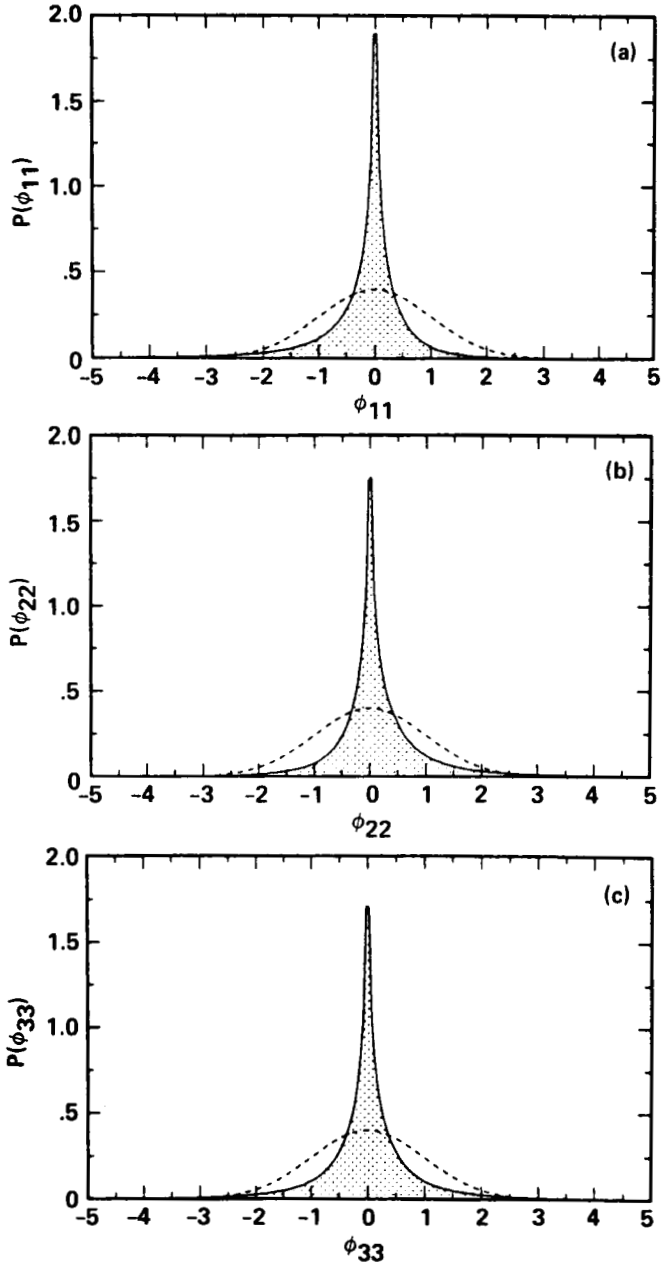

FIGURE 4. Pdf's of the diagonal elements of ϕ_{ij}: (*a*) $P(\phi_{11})$; (*b*) $P(\phi_{22})$; (*c*) $P(\phi_{33})$. ----, Gaussian distribution.

integrating the pdf of ϕ weighted by nth power of ϕ:

$$\overline{\phi^n} = \int_{-\infty}^{\infty} \phi^n \mathsf{P}(\phi)\, d\phi. \tag{10}$$

In order to evaluate the relative contributions to the mean value $\Phi_{\alpha\alpha} = \overline{\phi_{\alpha\alpha}}$ from different ranges of $\phi_{\alpha\alpha}$, the *weighted pdf* defined as $\phi_{\alpha\alpha}\mathsf{P}(\phi_{\alpha\alpha})$ is shown in figure 5 (the subdivisions are discussed below). The long tail in the *negative* ϕ_{11} region (ϕ_{11}^-) in figure 5(a) indicates that there is a substantial amount of energy leaving u in high-magnitude events, say, $\phi_{11}/\phi'_{11} < -1.5$ (see also figure 4a). On the other hand, figure 5(b) indicates that events with high-magnitude *positive* ϕ_{22} (ϕ_{22}^+) dominate in transferring energy into v (say $\phi_{22}/\phi'_{22} > 1.5$). However, both positive and negative ϕ_{33} events (ϕ_{33}^+, ϕ_{33}^-) equally contribute to the average Φ_{33} in the high-magnitude regions (say $|\phi_{33}/\phi'_{33}| > 1.5$, figure 5$c$). Also note that a considerable contribution to the statistical averages comes from low-magnitude events, $|\phi_{\alpha\alpha}/\phi'_{\alpha\alpha}| < 1.5$ (see §3.3 for a discussion).

The decomposition of the pressure–strain-rate introduced in §2.2 is applied to the weighted pdf. In figure 5, the height within each band denoted by a sign triplet shows the weighted pdf of $\phi_{\alpha\alpha}$ belonging to the corresponding class, and the area in that band represents contribution to the average from the class. For example, in figure 5(a), the area in the band $(-++)$ represents Φ_{11}^{-++} from class $\mathbf{C}^{-++}$ (in which $\phi_{11} < 0$, $\phi_{22} > 0$, $\phi_{33} > 0$):

$$\Phi_{11}^{-++} = \int_{-\infty}^{\infty} \phi_{11}\mathsf{P}(\phi_{11}^{-++})\, d\phi_{11}. \tag{11}$$

It is apparent that, in the low-magnitude regions, all the six classes of intercomponent energy transfer events play a significant role. However, high-magnitude portions (the tails of the weighted pdf's) are always dominated by only one class of events. In all, four classes of events dominate at high magnitudes — the same four classes listed in (9) on the basis of high-magnitude $\phi_{\alpha\alpha}$ contours.

Close agreement can be found between the high-magnitude portions of the pdf's and the local processes shown in figures 2 and 3. In the ϕ_{11}^- tail (figure 5a), for example, $\mathbf{C}^{-++}$ events are the major contributor. Similarly, the $\mathbf{C}^{-+-}$ events dominate in the ϕ_{22}^+ tail of figure 5(b), and $\mathbf{C}^{++-}$ and $\mathbf{C}^{--+}$ events, respectively, in the ϕ_{33}^- and ϕ_{33}^+ tails of figure 5(c).

3.3. *Relative significance of high- and low-magnitude events*

In contrast with the concentration of pressure–strain-rate events with high magnitude in figure 2, it is clear from the weighted pdf's (figure 5) that the net contribution of these powerful events to the statistical average is not necessarily dominant. This is because these events are concentrated in regions of very small volume and tower over a vast 'sea' of low-magnitude fluctuations whose total contribution to the average is as significant (figure 4). It is also clear from the previous discussions that the character of the high- and low-magnitude events is quite different. Indeed,

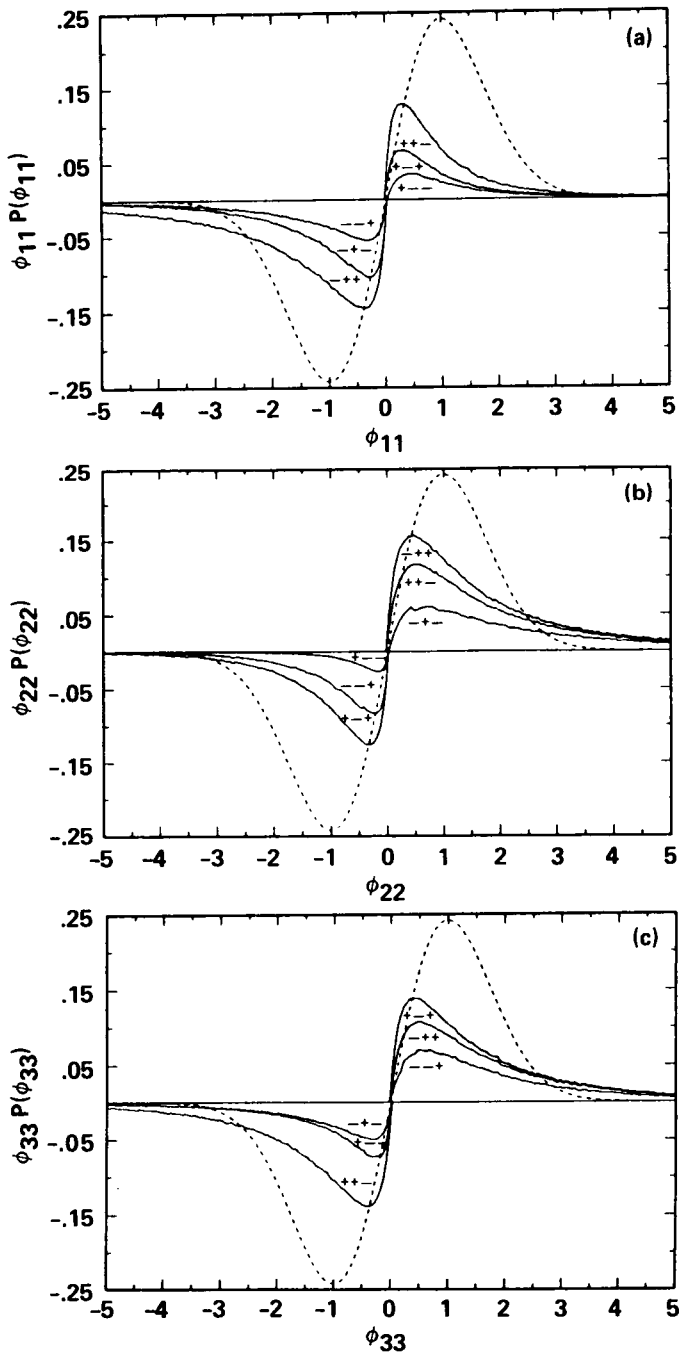

FIGURE 5. Weighted pdf's of the diagonal elements of ϕ_{ij}: (*a*) $\phi_{11}\mathsf{P}(\phi_{11})$; (*b*) $\phi_{22}\mathsf{P}(\phi_{22})$; (*c*) $\phi_{33}\mathsf{P}(\phi_{33})$. ----, weighted pdf for Gaussian distribution. The height within each band denoted by a sign triplet shows the weighted pdf of $\phi_{\alpha\alpha}$ belonging to the corresponding class, and the area in that band represents contribution to the average from the class.

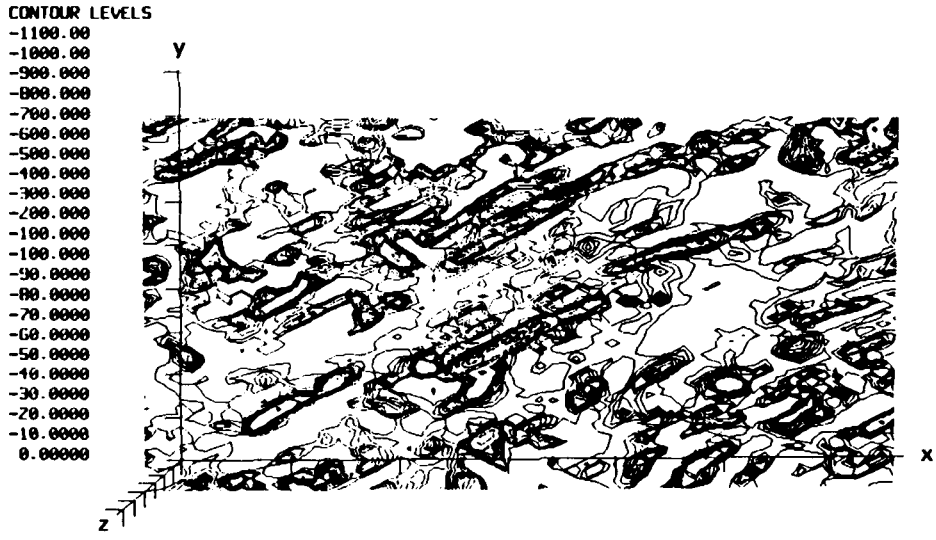

FIGURE 6. Contours of ϕ_{11} as in figure 2(a) with contours below $\phi_{11} = 100$ added. Note that countour increments below $\phi_{11} = 100$ are one-tenth of those above 100.

there is evidence that the powerful events are associated with the local coherent structure of the vorticity field (see BL).

Figure 6 shows contours of constant ϕ_{11} as in figure 2(a), but includes low-level contours below 100 (1.5 r.m.s.), the lowest level in figure 2(a). Note that the contour increment is 10 times smaller below $|\phi_{11}| = 100$ than above 100. Clearly, there is a great deal of low-magnitude activity which does not appear in figure 2(a). It turns out that the relative contribution to the average of the high-magnitude events (arbitrarily defined by the cutoff at 1.5 r.m.s) in each of the four dominant classes discussed above is roughly 50%. In other words, the high- and low-magnitude events contribute almost equally to the averages.

The statistical averages within each class of events, calculated by integrating the weighted pdf's in each band *over all magnitudes* of ϕ_{ij}, are schematically shown in figure 7. The same characteristics as in figure 3 can be found in this figure, i.e. most of energy transfer is carried out within the same four classes of events. Differences in detail, we speculate, are associated with the contributions of the low-magnitude ϕ_{ij} fluctuations to the averages.

Inspection of the energy transfer patterns in figure 7 poses an interesting question about the kinematic structure of the flow regimes involving intercomponent energy transfer. It appears that there is a common pattern of energy exchange in the all classes: the dominant energy transfer to or from one component is provided equally by the other two components. Does this mean that energy is exchanged axisymmetrically? If the off-diagonal terms in ϕ_{ij} (equivalently, s_{ij}) are negligible,

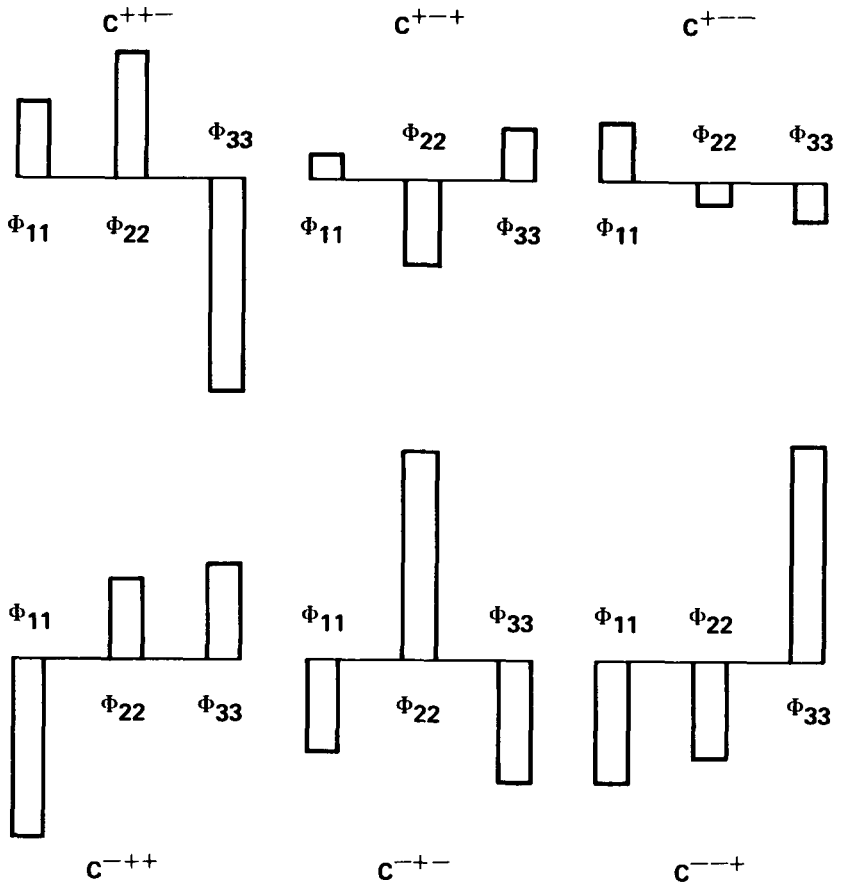

FIGURE 7. Schematic of the intercomponent energy transfer processes, representing the contributions from all magnitudes of ϕ_{ij} events, i.e. integration of the weighted pdf's in figure 5. The schematic also shows that the four classes $\mathbf{C}^{++-}$, $\mathbf{C}^{-++}$, $\mathbf{C}^{-+-}$ and $\mathbf{C}^{--+}$ are dominant (see figure 3).

then most of the energy transfer takes place within axisymmetric flow regimes, either 'rod-like' or 'disk-like' type. The answer awaits invariant analysis of the tensorial characteristics of the pressure–strain-rate (and strain rate).

4. Concluding remarks

Although a great deal has been learned about the process of intercomponent energy transfer as described by pressure–strain-rate correlations, many questions await further analysis. The most nagging of these questions regards the determination of 'significance.' It is clear, for example, that powerful pressure–strain-rate

events in which a great deal of energy transfer takes place locally in space exist; the pdf's of ϕ_{11}, ϕ_{22} and ϕ_{33} are extremely peaked around zero and possess very high flatness factors. It is because these events are so sparse that the net contributions to the statistical averages from the high-magnitude fluctuations are only 50% or less.

The *significance* of these powerful events in the evolution of the intercomponent energy transfer process, however, may be only partially related to their contribution to the statistical average. Indeed, the description of the qualitative features of the intercomponent energy transfer process as a whole by the high-magnitude events alone suggests that these powerful events may provide a major influence to the pressure–strain-rate fluctuations at all magnitudes. Currently in process is the development of schemes for isolation of the powerful events from the datasets through objective criteria, and further analysis of the separated datasets for determination of 'significance.'

Detailed analyses into the structure of powerful intercomponent energy transfer events, and their structural interrelationships with the local vorticity field are described in BL. We found that the energy transfer event Ⓐ in figure 2 is associated with a local stagnation point of high strain-rate and zero vorticity, apparently induced by a hairpin-vortex-type structure surrounding it. This event occurs in a region of *positive* slow pressure. Another powerful event with similar energy transfer characteristics was since found, which is associated with *negative* slow pressure. This event lies embedded within the legs of a hairpin vortex, suggesting that both events are associated with a vortical structure.

We briefly mention that the same analyses as described above have been applied to the rapid pressure–strain-rate term π_{ij} and results qualitatively similar to those for ϕ_{ij} have been found.

The authors wish to thank R. J. Adrian, J. C. R. Hunt, J. Kim, S. K. Lele, N. N. Mansour, P. Moin, R. S. Rogallo and M. M. Rogers for many helpful discussions during the 1988 Summer Program of the Center for Turbulence Research. J.G.B. gratefully acknowledges support from the Center for Turbulence Research and AFOSR.

REFERENCES

BRASSEUR, J. G. & LEE, M. J. 1987 Local structure of intercomponent energy transfer in homogeneous turbulent shear flow. In *Proc. 1987 Summer Program*, Center for Turbulence Research Report CTR–S87, NASA-Ames Research Center, pp. 165–178. [Referred to as BL in the text.]

HARRIS, V. G., GRAHAM, J. A. H. & CORRSIN, S. 1977 Further experiments in nearly homogeneous turbulent shear flow. *J. Fluid Mech.* **81**, 657–687.

KIM, J., MOIN, P. & MOSER, R. D. 1987 Turbulence statistics in fully-developed channel flow at low Reynolds number. *J. Fluid Mech.* **177**, 133–166.

LEE, M. J., KIM, J. & MOIN, P. 1987 Turbulence structure at high shear rate.

Sixth Symp. on Turb. Shear Flows, Toulouse, France, Sept 7-9, 1987, pp. 22.6.1–22.6.6.

LEE, M. J. & REYNOLDS, W. C. 1985 Numerical experiments on the structure of homogeneous turbulence. *Dept. Mech. Engng. Rep.* TF–24, Stanford University: Stanford, California.

LUMLEY, J. L. 1978 Computational modeling of turbulent flows. *Adv. Appl. Mech.* **18**, 123–176.

ROGALLO, R. S. 1981 Numerical experiments in homogeneous turbulence. NASA *Tech. Memo.* 81315.

ROGERS, M. M. & MOIN, P. 1987 The structure of the velocity field in homogeneous turbulent flows. *J. Fluid Mech.* **176**, 33–66.

ROGERS, M. M., MOIN, P. & REYNOLDS, W. C. 1986 The structure and modeling of the hydrodynamic and passive scalar fields in homogeneous turbulent shear flow. *Dept. Mech. Engng. Rep.* TF–25, Stanford University: Stanford, California.

TAVOULARIS, S. & CORRSIN, S. 1981 Experiments in nearly homogeneous turbulent shear flow with uniform mean temperature gradient. *J. Fluid Mech.* **104**, 311–347.